Nanoscale

RSC Publishing

PAPER

View Article Online
View Journal | View Issue

Cite this: *Nanoscale*, 2013, **5**, 12335

Core–shell Zn_2GeO_4 nanorods and their size-dependent photoluminescence properties†

Songping Wu,*[a] Zhuolin Wang,[a] Xin Ouyang[a] and Zhiqun Lin*[b]

Received 3rd September 2013
Accepted 3rd October 2013

DOI: 10.1039/c3nr04638a

www.rsc.org/nanoscale

Size-tunable crystalline core–crystalline shell Zn_2GeO_4 nanorods were synthesized *via* a facile hydrothermal reaction. High purity Zn_2GeO_4 nanorods were obtained at pH = 7. The length of Zn_2GeO_4 nanorods (L = 50–100 nm) can be controlled through a one-step process, while micro-sized nanorods with an aspect ratio of the length to the diameter of 10 were yielded in a two-step process. The single crystalline nature of Zn_2GeO_4 nanorods with a core–shell structure was verified by high resolution transmission electron microscopy (HRTEM) and selected area electron diffraction (SAED) measurements. The Raman study revealed that there is no oxygen defect ($V_O^{\cdot}$) in Zn_2GeO_4 nanocrystals, suggesting that photoluminescence emission of Zn_2GeO_4 can be attributed to the presence of the interstitial Zn defect ($Zn_i^{\cdot}$) in Zn_2GeO_4 nanocrystals. As the diameter of nanorods decreased, the excitation and emission peaks appeared to be redshifted due to the quantum size effect.

Introduction

Zn_2GeO_4 nanomaterials have attracted great attention as important functional materials for applications in electrochemical sensors, electronic devices, optical devices and catalysts. For example, RuO_2-dispersed Zn_2GeO_4 is a stable photocatalyst for water splitting.[1] Zn_2GeO_4 nanocrystals with a one-dimensional (1D) hexagonal structure possess superior photocatalytic activities to decompose a water–methanol solution into hydrogen under UV irradiation.[2] Zn_2GeO_4–ethylenediamine hybrid nanoribbon membranes exhibit an excellent recyclability and high selectivity for highly efficient removal of heavy metal ions from contaminated water.[3] Moreover, Zn_2GeO_4 can be utilized as a candidate for high-capacity anodes in lithium batteries.[4] They are also dielectric ceramics with excellent microwave properties[5] and high conductivity electrolytes.[6] The Mn-doped Zn_2GeO_4 (*i.e.*, Zn_2GeO_4:Mn) shows green luminescence, and can be employed for alternating-current thin-film electroluminescence devices.[7,8] Zn_2GeO_4 particles display white-bluish emission, and their photoluminescence (PL) is brighter than that of ZnO phosphor.[9] The PL peaks of Zn_2GeO_4 are located at 421 nm,[10] 470 nm,[11] 519 nm,[2] and 290 nm,[12] depending largely on the synthesis methods. It is worth noting that the size-dependent PL properties of Zn_2GeO_4 nanorods have not yet been reported.

Typical synthesis methods for Zn_2GeO_4 particles include conventional solid-state reaction,[1,13] vapor growth techniques,[12] hydrothermal synthesis,[9,14] surfactant-assisted hydrothermal synthesis,[15] solvothermal reaction,[2b,11] hydrolysis of alkoxides,[16] and aqueous processes.[17] Among them, the hydrothermal method stands out as an effective strategy to produce Zn_2GeO_4 nanorods. Notably, crystalline Zn_2GeO_4 particles can be easily synthesized through the solid-state method.[1,12] Recently, Zn_2GeO_4 nanorods composed of a crystalline core–amorphous shell have been prepared.[3,9] However, core–shell Zn_2GeO_4 nanorods with both the core and shell being crystalline have not yet been reported. Herein, we report the synthesis of size-tunable crystalline core–crystalline shell Zn_2GeO_4 nanorods *via* a facile hydrothermal reaction. Interestingly, the length of Zn_2GeO_4 nanorods (L = 50–100 nm) can be readily controlled through a one-step process, while micro-sized nanorods with an aspect ratio of the length to the diameter of 10 were yielded in a two-step process. The HRTEM and SAED measurements confirmed the single crystalline nature of core–shell Zn_2GeO_4 nanorods. The Raman experiment revealed no oxygen defect ($V_O^{\cdot}$) in Zn_2GeO_4 nanocrystals, signifying that the PL emission of Zn_2GeO_4 nanorods can be attributed to the presence of the interstitial Zn defect ($Zn_i^{\cdot}$) in Zn_2GeO_4 nanocrystals. Quite intriguingly, as the diameter of nanorods decreased, the excitation and emission peaks red-shifted due to the quantum size effect.

Experimental section

All chemicals, including $Zn(NO_3)_2 \cdot 6H_2O$ (AR, Aladdin, Shanghai, China) and GeO_2 (≥99.9%; Aladdin, Shanghai, China), were used as received without further purification. A one-step process to yield Zn_2GeO_4 nanorods (L = 50–100 nm)

[a]*School of Chemistry and Chemical Engineering, South China University of Technology, Guangzhou, 510641, China. E-mail: chwsp@scut.edu.cn; Fax: +86-20-87112897; Tel: +86-20-87112897*

[b]*School of Materials Science and Engineering, Georgia Institute of Technology, Atlanta, Georgia 30332, USA. E-mail: zhiqun.lin@mse.gatech.edu; Tel: +1 404 385 4404*

† Electronic supplementary information (ESI) available. See DOI: 10.1039/c3nr04638a

was conducted as follows. Firstly, 2 mmol $Zn(NO_3)_2 \cdot 6H_2O$ was dissolved in 60 ml distilled water, and then 1 mmol GeO_2 were added to the solution under constant magnetic stirring for 30 min at room temperature. NaOH or HCl solution (1 mol l^{-1}) was then added to the above uniform solution to adjust pH. Cetyltrimethyl ammonium bromide (CTAB) was used to adjust the morphology and the size of the resulting Zn_2GeO_4. Finally, the mixture was transferred into a Teflon-lined stainless steel autoclave with an inner volume of 80 ml. The autoclave was sealed and placed in a digital-type temperature-controlled oven at an appropriate temperature for several hours. After the reaction was complete, the solution was cooled down to room temperature. The product was filtered out and washed with distilled water several times. The final powder was dried at 60 °C overnight. For a two-step process that yielded micro-sized Zn_2GeO_4 nanorods with an aspect ratio of the length to the diameter of 10, 2 mmol GeO_2 was dispersed in 60 ml distilled water. NaOH was then added to control pH = 10 under constant magnetic stirring for 30 min at room temperature. Finally, the mixture was transferred into the above-mentioned autoclave, and hydrothermally reacted at 250 °C for 8 h to yield single crystal $Na_4Ge_9O_{20}$. 0.1 mmol $Na_4Ge_9O_{20}$ was reacted with 0.18 mmol $ZnNO_3 \cdot 6H_2O$ at pH = 7 at various temperatures for 8 h to form micro-sized Zn_2GeO_4 nanorods. Zn_2GeO_4 particles were also synthesized by the solid-state method according to our previous work[5] and served as the control.

The crystalline phases of samples were analyzed by X-ray diffraction (XRD) (D8 Advance, Bruker, Germany) with Cu Kα radiation (2θ = 10–65°). Transmission electron microscopy (TEM), high-resolution TEM (HRTEM) and selective area electron diffraction (SAED) images were taken with a JEM-2100HR electron microscope (JEOL, Tokyo, Japan) with an accelerating voltage of 200 kV, which was also employed to corrode Zn_2GeO_4 nanorods for the investigation of their core–shell structures. FT-IR and Raman spectra of Zn_2GeO_4 nanorods were obtained using a Fourier transform infrared spectrometer (Vector 33, Brucker, Germany) and Micro-Raman spectrometer (LabRAM Aramis, HJY, France), respectively. The photoluminescence (PL) spectra and their excitation (photoluminescence excitation: PLE) spectra were measured using a fluorescence spectrometer (F-4500, Hitachi, Japan).

Results and discussion

In this work, pH was found to play an important role in preparing Zn_2GeO_4 nanocrystals. Fig. 1 shows XRD patterns of the samples synthesized at different pH values at 250 °C for 72 h. Clearly, at pH = 2 the main crystal phase was from raw material GeO_2 (JCPDS no. 36-1643), accompanied by a trace of Zn_2GeO_4 (JCPDS no. 11-0687). The amount of rhombohedral Zn_2GeO_4 increased as the pH increased. The pure rhombohedral phase of Zn_2GeO_4 was yielded at pH = 7. It is worth noting that argutite tetragonal GeO_2 (JCPDS no. 35-0729) appeared at pH = 4–6, suggesting the variety of GeO_2 formed at these pH values. In addition, a competitive reaction occurred at pH = 5 and produced ZnO (JCPDS no. 36-1451). At pH ≥ 8, $Zn(OH)_2$ (JCPDS no. 12-0142) was found to coexist in the product.

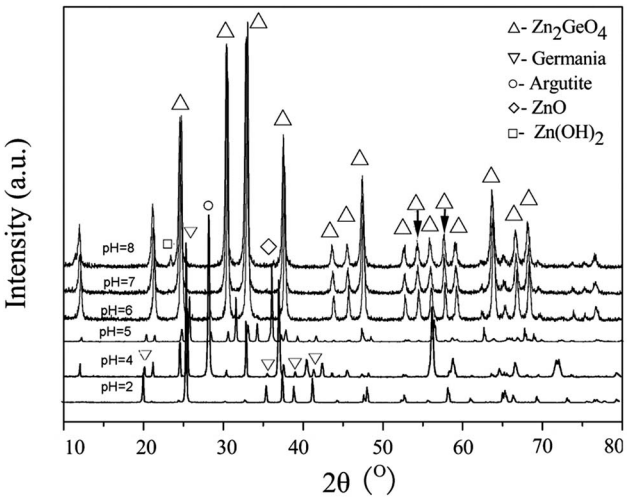

Fig. 1 XRD patterns of Zn_2GeO_4 nanocrystals synthesized at different pH values at 250 °C for 72 h.

The high-magnification TEM images (Fig. 2a and d) revealed that these Zn_2GeO_4 nanorods synthesized at 250 °C were approximately 40 nm in diameter. The nanorods possessed smooth surfaces and semi-circular closed tips. The lattice fringe of the (113) plane with an interplanar spacing of 0.29 nm was observed at an angle of 66° to the rod direction (Fig. 2b). The uniform lattice fringe (Fig. 2b) and the corresponding FFT pattern (inset in Fig. 2b) and a spot-like pattern of selected area electron diffraction (SAED) (Fig. 2c) of the Zn_2GeO_4 nanorods substantiated that each nanocrystal comprised a single crystalline domain.[11]

In contrast to amorphous outer layers (*i.e.*, shells) observed in Ge nanowires,[18] silicon carbide nanowires,[19] silicon nitride nanowires,[20] Zn_2GeO_4 nanorods[21] and nanoribbons,[3] in this work core–shell Zn_2GeO_4 nanorods with both the crystalline core and crystalline shell were observed. The outer layer (*i.e.*, the shell) has a spacing of 0.29 nm (Fig. 2e, h and j), corresponding to the (113) lattice plane. Moreover, several disconnections at the core–shell interface can be seen in Fig. 2d and e. To further elucidate the core–shell structure and the growth of Zn_2GeO_4 nanorods, we employed the high-energy electron beam from HRTEM to corrode nanorods, and found that the nanorod shell was very easy to volatilize. The electrochemical corrosion is clearly evident on the surface of Zn_2GeO_4 nanorods, where the cores were exposed (Fig. 2f and j). The exposed core has lattice spacings of 0.71 nm and 0.29 nm (Fig. 2h), corresponding to that of (110) and (113) lattice planes of the rhombohedral phase of Zn_2GeO_4, respectively. However, the exposed core has lattice spacings of 0.41 nm and 0.29 nm (Fig. 2j) for the specimen synthesized (at 6% weight ratio of CTAB/Zn_2GeO_4) at 150 °C for 6 h, corresponding to the (300) and (113) lattice planes, respectively. Clearly, the core–shell structure can be observed in different specimens synthesized under various conditions (Fig. 2a and d–j). We thus conclude that Zn_2GeO_4 nanorods grew along the *c* axis of the rhombohedral phenacite-type structure.[2a,11,22]

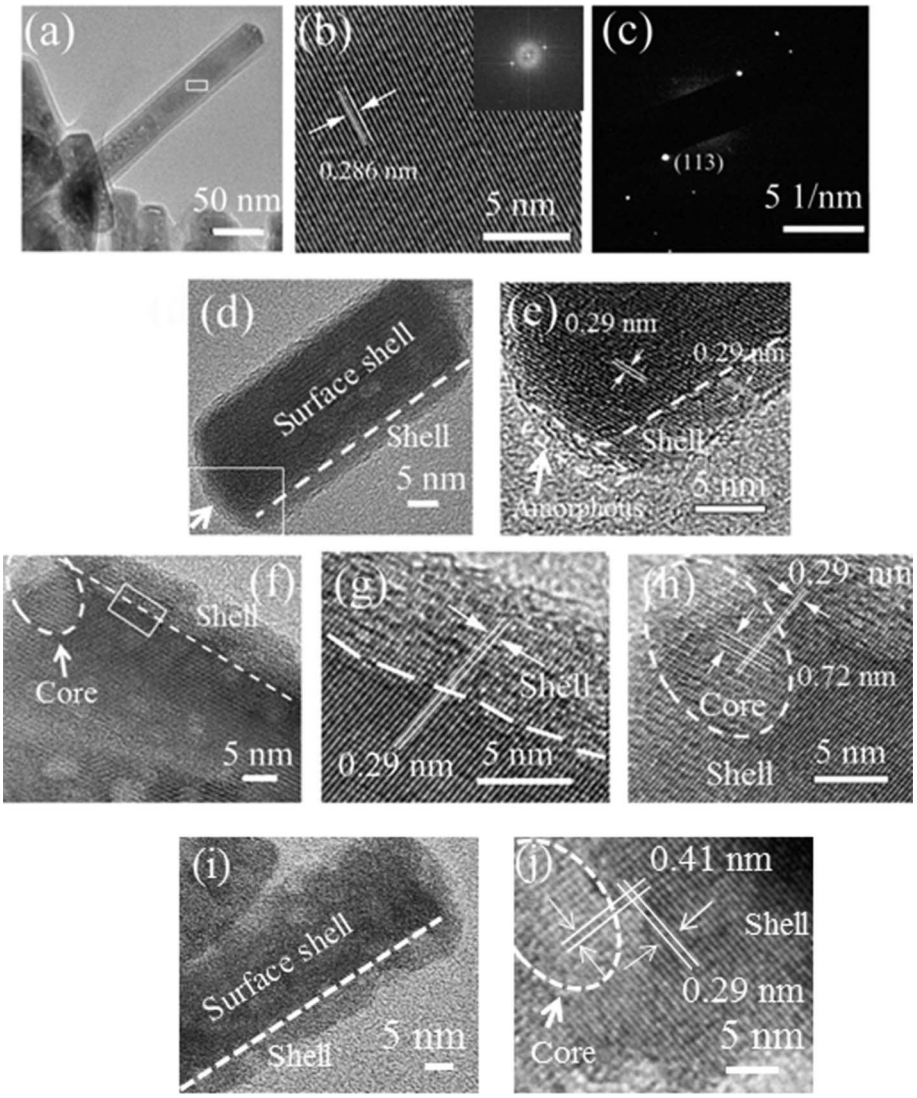

Fig. 2 (a) A representative TEM image of Zn_2GeO_4 nanorods. (b) A HRTEM image of the close-up marked as a white box in (a), and the corresponding FFT pattern is shown in the inset. (c) The corresponding SAED pattern of a long nanorod in (a). (d–f) HRTEM images of Zn_2GeO_4 nanorods; (e) the close-up marked as a white box in (d); (g) and (h) the close-ups marked as a white box and a dashed circle in (f), respectively. (a–e) Zn_2GeO_4 nanorods were synthesized at pH = 7 at 250 °C for 4 h. (f, i and j) Zn_2GeO_4 nanorods were synthesized at pH = 7 at 150 °C for 1 h at the weight ratios of CTAB to Zn_2GeO_4 of 4.0, 0.01 and 0.06, respectively.

The formation of crystalline core–crystalline shell Zn_2GeO_4 nanorods may be rationalized as follows. Crystalline Zn_2GeO_4 first appeared as the core with (113) and (110) or (300) planes. Non-crystalline $Zn(OH)_2/Ge(OH)_4$ were then absorbed on the core surface and formed the outer layer (*i.e.*, the shell). The non-crystalline outer layer slowly crystallized as the reaction progressed, and finally became the crystalline Zn_2GeO_4 shell with the (113) plane. The periodic bond chain theory predicts that the (110) plane is parallel to the *c* axis, which is considered to be energetically more stable than the (113) plane in crystallography.[2a,22] As a result, new crystals of Zn_2GeO_4 would preferentially grow through the (113) plane. As evidenced in Fig. 2d and e, an amorphous layer (marked with an arrow) still existed at the tip of the nanorod. This is not surprising as the domain was not in the plane (113) of the nanorod.

FTIR spectra of Zn_2GeO_4 nanorods are shown in Fig. 3a, where the absorption ranges of Zn_2GeO_4 are located at 535 cm^{-1} and 743–801 cm^{-1}, correlating well with the characteristic infrared absorption ranges of Zn_2GeO_4 (*i.e.*, $\nu(ZnO_4)$ 500–600 cm^{-1} and $\nu(GeO_4)$ 700–800 cm^{-1}) in the literature.[16] The local atomic structures of Zn_2GeO_4 nanorods were revealed by Raman spectroscopy (Fig. 3b). It has been reported that Raman peaks at 748 cm^{-1}, 754 cm^{-1}, and 778 cm^{-1} are attributed to Ge–O–Zn symmetric, defect oxygen mode, and Ge–O–Zn asymmetric vibrations, respectively.[21] The peak at 754 cm^{-1} was clearly evident for the sample prepared by the solid-state method.[6] However, this peak became too weak to be detected for the samples synthesized by the hydrothermal route, suggesting that there is no oxygen defect in the as-prepared Zn_2GeO_4 nanorods.

We note that in this work the morphology and size of Zn_2GeO_4 nanorods can be controlled by adjusting the reaction conditions (*i.e.*, the reaction temperature, time, and the use of surfactant) and reaction process. The influence of the reaction temperature on the phase of the resulting Zn_2GeO_4 nanorods is

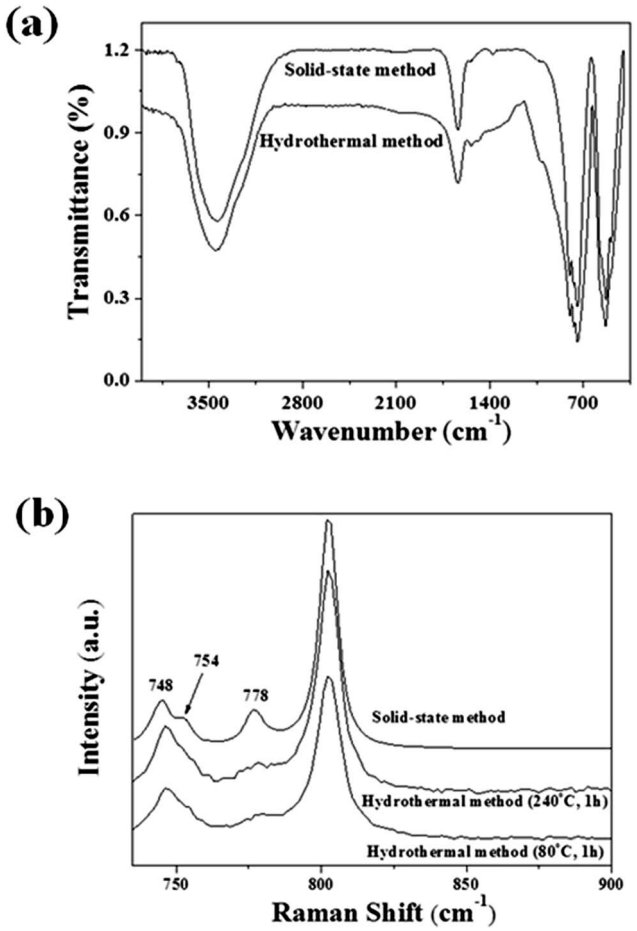

Fig. 3 (a) FTIR and (b) Raman spectra of Zn_2GeO_4 nanorods prepared by different methods.

shown in Fig. 4a. Clearly, pure rhombohedral Zn_2GeO_4 with approximately 20 nm crystalline size (calculated by the Scherrer equation) formed for all samples, regardless of the reaction temperatures, suggesting that rhombohedral Zn_2GeO_4 has a very wide reaction temperature region at pH = 7. A large amount of pure Zn_2GeO_4 nanorods with 50–100 nm length was observed (Fig. 4b–f). The length of Zn_2GeO_4 nanorods increased with the increase in reaction temperature, while the aspect ratio of the length to the diameter of final nanorods was nearly unchanged ($L/D = \sim 3$). The average length of the as-prepared Zn_2GeO_4 nanorods was roughly 53 nm (Fig. 4b) at 180 °C. It then increased gradually as the temperature was increased. Zn_2GeO_4 nanorods with a length of 86 nm and a diameter of 30 nm were yielded at 250 °C (Fig. 4e). The size and morphology of Zn_2GeO_4 nanorods did not change obviously with a further increase in the reaction temperature (*i.e.*, 270 °C; Fig. 4f). During the crystal growth, the size and morphology of the final product depend on the competition between the crystal nucleation and the crystal growth, which is dictated by the delicate balance between the growth thermodynamics and the growth kinetics. As a direct consequence, in this work desirable size-controlled nanorods were obtained by changing the growth conditions. The high reaction temperature appears beneficial to the formation of large nanorods.

Surfactants such as poly(ethylene glycol) (PEG),[11] CTAB[23,24] or amino acids[25] have been shown to exert a profound influence on the morphology and size of nanoparticles. In this work the cationic surfactant CTAB was employed to adjust the size of Zn_2GeO_4 hydrothermally synthesized at 150 °C for 6 h as shown in Fig. 5. Although nanorods were found to exist in all samples regardless of the amount of CTAB used, the length and aspect ratio of nanorods decreased as the amount of CTAB increased (Fig. 6). In this work, the thickness of the shell in core–shell Zn_2GeO_4 nanorods was in the range of 4–6 nm, as shown in Fig. S1 and S2.† It is well known that spherical micelles are dominant in a CTAB solution, in which the micelle concentration is slightly higher than its critical micelle concentration (CMC = ~1 mM), while worm-like micelles are predominant at higher concentrations (c_{CTAB} > CMC).[26,27] In the present study, at c_{CTAB} = 4%, these worm-like micelles with which the nanorods are templated (the central panel in Scheme 1) break into short cylindrical micelles under hydrothermal conditions (the right panel in Scheme 1).[28,29] The change of cylindrical micelles into spherical micelles is driven by lower surface energy as the amount of CTAB increases. However, the number of surface hydroxyl groups on nanorods was limited at pH = 7; thus the micelles are not tightly bound with negatively charged nanorods,[23] thereby leading to short cylindrical nanorods instead of spherical nanoparticles as illustrated in Scheme 1.

We now turn our attention to the two-step process with which micro-sized nanorods with a length up to 1 μm and a large aspect ratio were obtained. We first synthesized single crystal $Na_4Ge_9O_{20}$. In comparison with the single crystalline diffraction pattern of $Na_4Ge_9O_{20}$ shown in curve α (Fig. 7), several diffraction peaks cannot be observed in the powder diffraction pattern of $Na_4Ge_9O_{20}$ (curve β in Fig. 7) due to the obvious oriented growth on the surface of single crystal $Na_4Ge_9O_{20}$.[30] We note that $Na_4Ge_9O_{20}$ then reacted with $Zn(NO_3)_2 \cdot 6H_2O$ to yield micro-sized Zn_2GeO_4 nanorods, and their XRD pattern is given in curve γ (Fig. 7). The nanorods 500–600 nm long and 50 nm wide can be synthesized using a two-step process at 150 °C (Fig. 7b). As the temperature was increased to 250 °C, the length of nanorods further increased to a few micrometers with an aspect ratio of the length to the diameter of 8–10 (Fig. 7c). The HRTEM image of nanorods (Fig. 7d) shows a single crystalline structure (Fig. 7e). The lattice spacing of 0.334 nm corresponded well to that of the (220) lattice plane of the rhombohedral phase of Zn_2GeO_4. The FFT (the inset in the upper-right of Fig. 7e) and SAED patterns (Fig. 7f) further substantiated the formation of single crystals of Zn_2GeO_4 nanorods.

The photoluminescence properties of Zn_2GeO_4 nanorods were also explored. When the average diameter of Zn_2GeO_4 nanorods was less than 22 nm, the excitation spectra exhibited narrow peaks located around 287–293.8 nm (Fig. 8a), which is due to the excitation from the valence band to the conduction band of Zn_2GeO_4.[9] As reported in the literature, the excitation peaks located at 260 nm (ref. 9) or 290 nm (ref. 12) for Zn_2GeO_4 nanocrystals depend on different sample preparation methods. In this work as the diameter of Zn_2GeO_4 nanorods increased, a red shift of the excitation peak was observed due to the

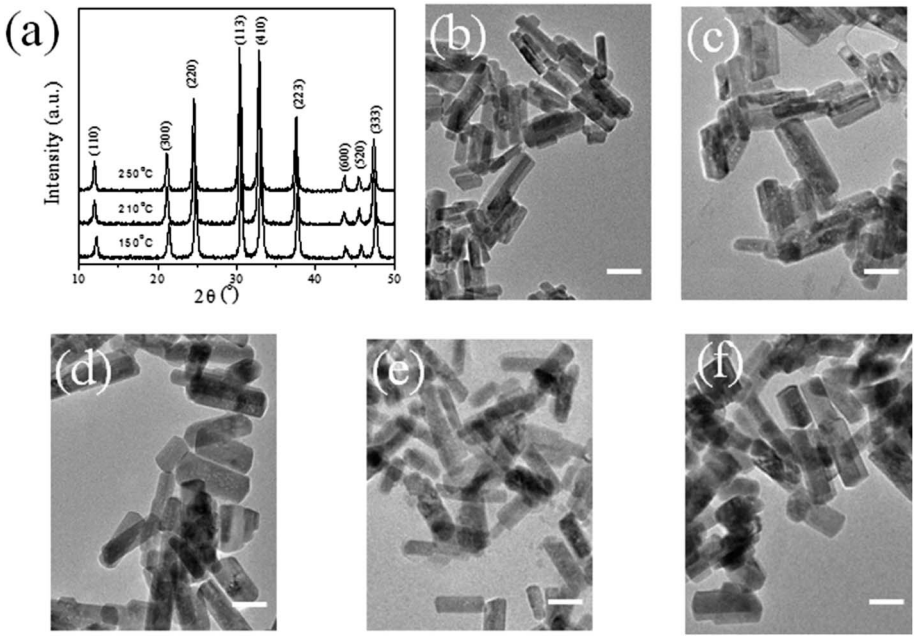

Fig. 4 (a) XRD patterns of Zn_2GeO_4 nanorods synthesized at different temperatures. TEM images of Zn_2GeO_4 nanorods synthesized at different temperatures for 1 h: (b) 180 °C, (c) 210 °C, (d) 240 °C, (e) 250 °C, and (f) 270 °C. Scale bars = 50 nm in all TEM images.

quantum confinement effect. Such Zn_2GeO_4 nanorods may be used as deep-ultraviolet (DUV) photodetectors operating in the solar blind spectrum range (220–290 nm).[31]

Photoluminescence (PL) spectra of Zn_2GeO_4 nanorods were located around 310–360 nm (Fig. 8b). A strong PL emission at 519 nm in the pure Zn_2GeO_4 phase at room temperature has been reported in the literature, and its origin was attributed to a donor–acceptor recombination process based on native defects, that is, $V_O^{\cdot}$ (oxygen-defect) and $Zn_i^{\cdot}$ (interstitial monovalent Zn) as donors, and V_{Ge} (Ge-related centers) and V_{Zn}'' (Zn-defect) as acceptors.[9] Moreover, it has been found that $Zn_i^{\cdot}$ is not essential for the luminescence as the Zn_2GeO_4 phase, where only $V_O^{\cdot}$ is detected by the electron spin resonance (ESR), showed the intensity of PL at 484 nm comparable to the phase in which both $V_O^{\cdot}$ and $Zn_i^{\cdot}$ were detected.[12] Notably, the presence of neutral-donor-bound exciton transitions in ZnO has been confirmed in the literature, and the neutral donors are the pair type complexes.[32] The PL spectra of ZnO films showed that near-band-edge emission had a shoulder at 3.382 eV and five distinct peaks. Among the PL peaks, the dominant emission peaks are

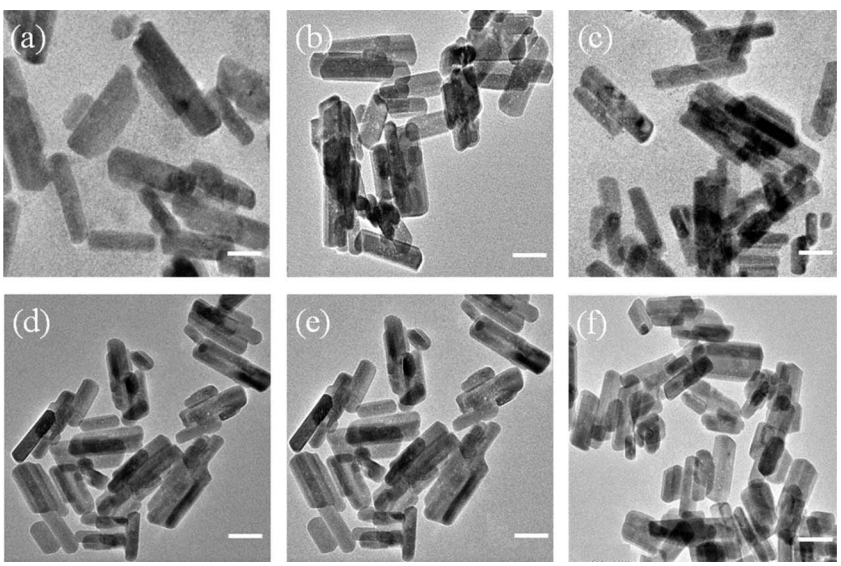

Fig. 5 TEM images of Zn_2GeO_4 nanorods synthesized at different weight ratios of $wt_{CTAB}/wt_{Zn2GeO4}$: (a) 0, (b) 0.5, (c) 1.0, (d) 2.0, (e) 3.0, and (f) 4.0. Scale bars = 50 nm in all TEM images.

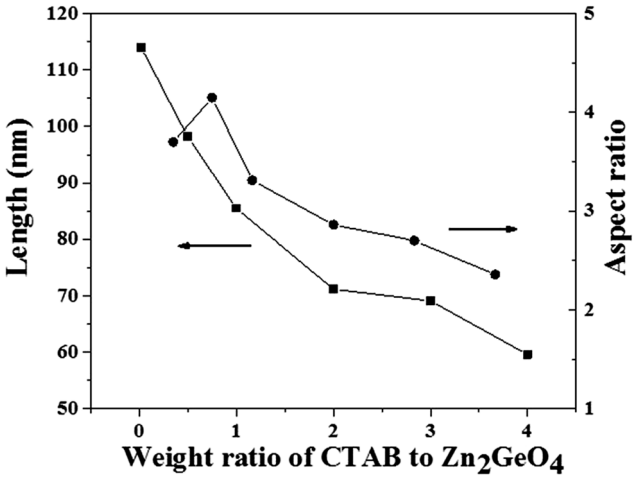

Fig. 6 Influence of CTAB on the length and the aspect ratio of Zn_2GeO_4 nanorods.

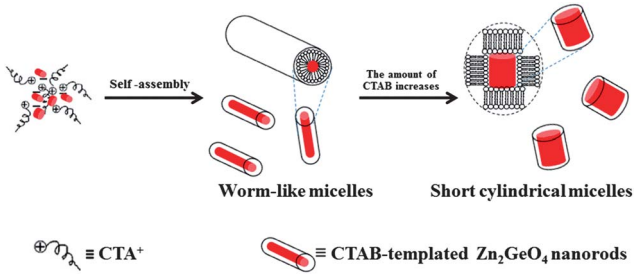

Scheme 1 A schematic illustration depicting different morphologies of nanorods in the CTAB micelle solution with various amounts of CTAB.

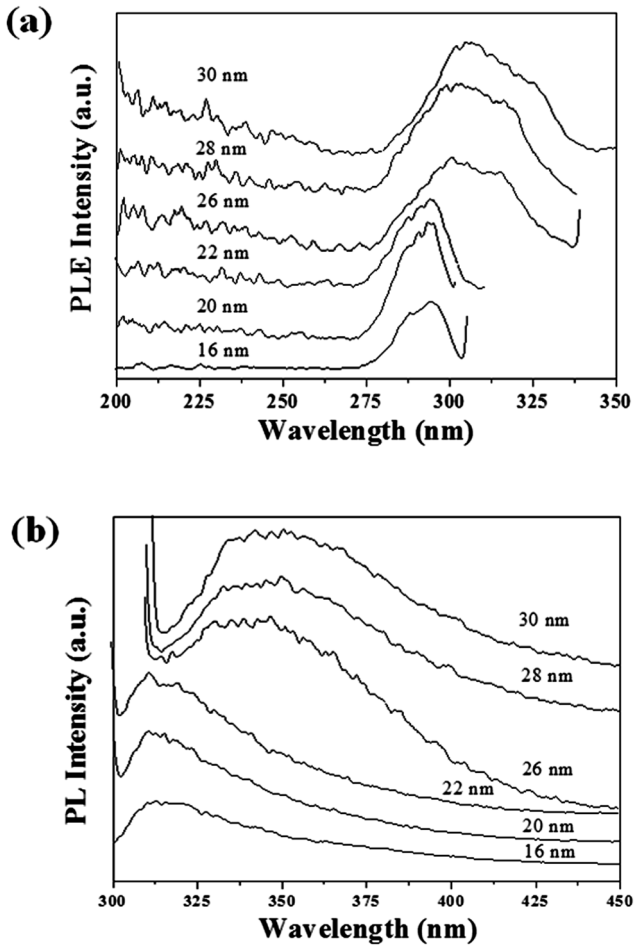

Fig. 8 (a) PLE and (b) PL spectra of Zn_2GeO_4 nanorods with different diameters.

due to the exciton transitions (D^0X) bound to neutral donors and their excited states.[33] For ZnO nanorods with ~100 nm diameter, both the spectral shape and peak position of band edge emission are affected by the concentration of defects.[34] In the present study, the emission peaks at ~310 nm can be attributed to exciton transitions bound to neutral donors and their excited states. Notably, defects in nanorods play an important role in the luminescence of Zn_2GeO_4 nanorods. As

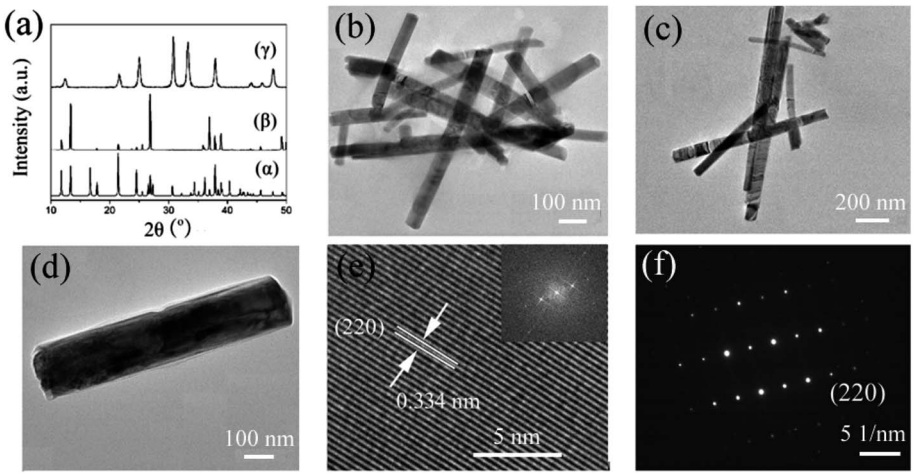

Fig. 7 (a) XRD patterns of the simulated pattern of $Na_4Ge_9O_{20}$ (curve α), $Na_4Ge_9O_{20}$ powders (curve β) and Zn_2GeO_4 nanorods (curve γ). TEM images of Zn_2GeO_4 nanorods synthesized by a two-step process at different temperatures for 1 h: (b) 150 °C, (c) 250 °C. (d) TEM, (e) HRTEM (inset: FFT pattern), and (f) the corresponding SAED image of Zn_2GeO_4 nanorods synthesized using a two-step process at 250 °C at pH = 7 for 4 h.

the Zn_2GeO_4 phase is structurally open, some of Zn ions may be incorporated into the six-membered rings due to the cation disorder. Therefore, the preferential formation of $Zn_i^{\cdot}$ was possibly accomplished in the nanocrystallized Zn_2GeO_4.[9,12] Thus, we speculate that the interstitial Zn defect ($Zn_i^{\cdot}$) in Zn_2GeO_4 exerts a marked influence on the emission of Zn_2GeO_4 due to the deficiency in defect oxygen as revealed by Raman measurements.

The increase in the diameter of nanorods would cause a redshift in the band edge emission due to the quantum confinement effect. It has been reported that ultrathin ZnO nanobelts with the thicknesses of 5.5 nm and 200 nm exhibited near band edge emissions at 373 nm and 387 nm, respectively.[35] The carriers may move freely in two-dimensional (2D) nanobelts. In contrast, in the case of 1D Zn_2GeO_4 nanorods the carriers only move freely along the long axis of nanorods. Thus, the size effect became more obvious when the diameter of 1D Zn_2GeO_4 nanorods varied.

Conclusions

In summary, Zn_2GeO_4 nanorods with tunable size have been synthesized through a hydrothermal route. Zn_2GeO_4 nanorods with 50–100 nm length and an aspect ratio of the length to the diameter of 3 were produced *via* a one-step process. In contrast, micro-sized nanorods (up to 1000 nm long and with a high aspect ratio of 10) can be yielded in a two-step process. The single crystalline nature of Zn_2GeO_4 nanorods with a crystalline core–crystalline shell structure was substantiated by HRTEM and SAED measurements. The interstitial Zn defect ($Zn_i^{\cdot}$) in Zn_2GeO_4 markedly affected the PL of Zn_2GeO_4 due to the lack of oxygen defect as revealed by Raman measurements. As the diameter of nanorods was decreased, both excitation and emission peaks red-shifted due to the quantum size effect.

Acknowledgements

This work was supported by the Guangdong-Hong Kong Technology Cooperation Funding Scheme (TCFS) under Grant 2010A090604002 and a China Scholarship.

References

1 J. Sato, H. Kobayashi, K. Ikarashi, N. Saito, H. Nishiyama and Y. Inoue, *J. Phys. Chem. B*, 2004, **108**, 4369.
2 (*a*) J. Liang, Y. Cao, H. Lin, Z. Zhang, C. Huang and X. Wang, *Inorg. Chem.*, 2013, **52**, 6916; (*b*) J. Liang, J. Xu, J. Long, Z. Zhang and X. Wang, *J. Mater. Chem. A*, 2013, **1**, 10622.
3 L. Yu, R. Zou, Z. Zhang, G. Song, Z. Chen, J. Yang and J. Hu, *Chem. Commun.*, 2011, **47**, 10719.
4 J. K. Feng, M. O. Lai and L. Lu, *Electrochem. Commun.*, 2011, **13**, 287.
5 S. Wu and Q. Ma, *J. Alloys Compd.*, 2013, **567**, 40.
6 S. Wu, Q. Ma and F. He, *J. Am. Ceram. Soc.*, 2013, **96**, 2046.
7 L. C. Williams, D. Norton, J. Budai and P. H. Holloway, *J. Electrochem. Soc.*, 2004, **151**, H188.
8 J. P. Bender, J. F. Wager, J. Kissick, B. L. Clark and D. A. Keszler, *J. Lumin.*, 2002, **99**, 311.
9 Z. Liu, X. Jing and L. Wang, *J. Electrochem. Soc.*, 2007, **154**, H500.
10 L. Z. Pei, Y. Yang, L. J. Yang, C. G. Fan, C. Z. Yuan and Q. Zhang, *Solid State Commun.*, 2011, **151**, 1036.
11 S. Takeshita, J. Honda, T. Isobe, T. Sawayama and S. Niikura, *Cryst. Growth Des.*, 2010, **10**, 4494.
12 Y. Takahashi, M. Ando, K. Iwasaki, H. Masai and T. Fujiwara, *Appl. Phys. Lett.*, 2010, **97**, 071906.
13 Y. Su, X. Meng, Y. Chen, S. Li, Q. Zhou, X. Liang and Y. Feng, *Mater. Res. Bull.*, 2008, **43**, 1865.
14 B. Ma, F. Wen, H. Jiang, J. Yang, P. Ying and C. Li, *Catal. Lett.*, 2010, **134**, 78.
15 C. Hung, M. Chang, C. Ho, C. Yu, W. Lin and Q. Zhang, *J. Electrochem. Soc.*, 2010, **157**, K80.
16 O. Yamaguchi, J. Hidaka and K. Hirota, *J. Mater. Sci. Lett.*, 1991, **10**, 1471.
17 M. Tsai, C. Yu, C. Wang and T. Perng, *Cryst. Growth Des.*, 2008, **8**, 2264.
18 L. W. Lin, Y. H. Tang, C. S. Chen and H. F. Xu, *CrystEngComm*, 2010, **12**, 2975.
19 W. Shi, Y. Zheng, H. Peng, N. Wang, C. S. Lee and S. Lee, *J. Am. Ceram. Soc.*, 2000, **83**, 3228.
20 X. C. Wu, W. H. Song, B. Zhao, W. D. Huang, M. H. Pu, Y. P. Sun and J. J. Du, *Solid State Commun.*, 2000, **115**, 683.
21 V. B. R. Boppana, N. D. Hould and R. F. Lobo, *J. Solid State Chem.*, 2011, **184**, 1054.
22 S. Yan, L. Wan, Z. Li and Z. Zou, *Chem. Commun.*, 2011, **47**, 5632.
23 Y. Zhou, Q. Zhang, J. Gong and S. Yu, *J. Phys. Chem. C*, 2008, **112**, 13383.
24 S. Chen, X. Chen, Z. Xue, J. Zhou, J. Li, J. Hong and X. You, *J. Mater. Chem.*, 2003, **13**, 1132.
25 T. Nguyen, D. Mrabet, T. Vu, C. Dinh and T. Do, *CrystEngComm*, 2011, **13**, 1450.
26 Z. Lin, *Langmuir*, 1996, **12**, 1729.
27 R. Bott, T. Wolff and K. Zierold, *Langmuir*, 2002, **18**, 2004.
28 E. Faetibold, B. Michels and G. Waton, *J. Phys. Chem.*, 1996, **100**, 20063.
29 T. H. Ha, Y. J. Kim and S. H. Park, *Chem. Commun.*, 2010, **46**, 3164.
30 K. B. Sundaram and A. Khan, *Thin Solid Films*, 1997, **295**, 87.
31 (*a*) L. Li, P. S. Lee, C. Yan, T. Zhai, X. Fang, M. Liao, Y. Koide, Y. Bando and D. Golberg, *Adv. Mater.*, 2010, **22**, 5145; (*b*) Z. Liu, B. Liang, G. Chen, G. Yu, Z. Xie, L. Gao, D. Chen and G. Shen, *J. Mater. Chem. C*, 2013, **1**, 131.
32 D. C. Reynolds, D. C. Look, B. Jogai, C. W. Litton, T. C. Collins, W. Harsch and G. Cantwell, *Phys. Rev. B: Condens. Matter Mater. Phys.*, 1998, **57**, 12151.
33 S. W. Jung, W. I. Park, H. D. Cheong, G.-C. Yi, H. M. Jang, S. Hong and T. Joo, *Appl. Phys. Lett.*, 2002, **80**, 1924.
34 J. Cui, *J. Phys. Chem. C*, 2008, **112**, 10385.
35 X. Wang, Y. Ding, C. J. Summers and Z. L. Wang, *J. Phys. Chem. B*, 2004, **108**, 8773.